# Stereoelectronic Switching in Single-Molecule Junctions

Timothy A. Su,[1] Haixing Li,[2] Michael L. Steigerwald,[1*] Latha Venkataraman,[2*] Colin Nuckolls[1*]

[1]Department of Chemistry, Columbia University, New York, New York 10027
[2]Department of Physics and Applied Math, Columbia University, New York, New York 10027

## Table of Contents

## I. Supplemental Figures from Main Text

**Figure S1**: 2D histograms of **Si1-Si3; Si5-Si10**. For measurements with **Si10**, we observe two high G peaks (apparent in Figure 3a) that are most probably due to the frequent formation of junctions with two molecules in parallel. The switching data presented in the 2D histogram for **Si10** below should then also describe switching events where two molecules in the low G state switch to two molecules in the high G state. This can be rationalized from the corresponding inset where the conductance profiles of the pre- and post-switching states are overlaid with the 1D conductance histogram of Figure 3a.
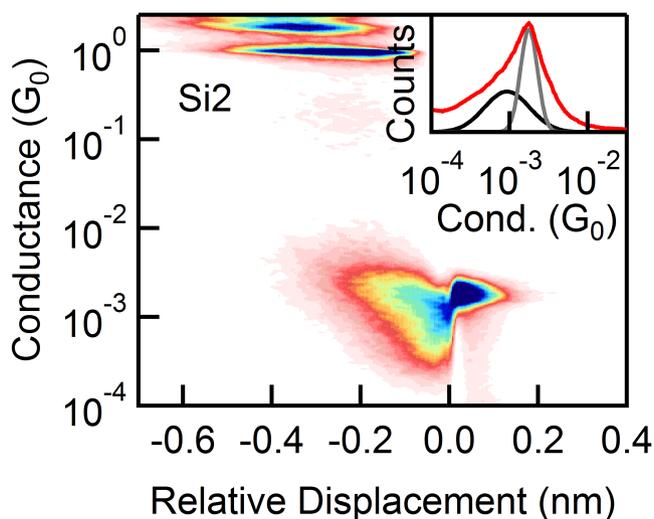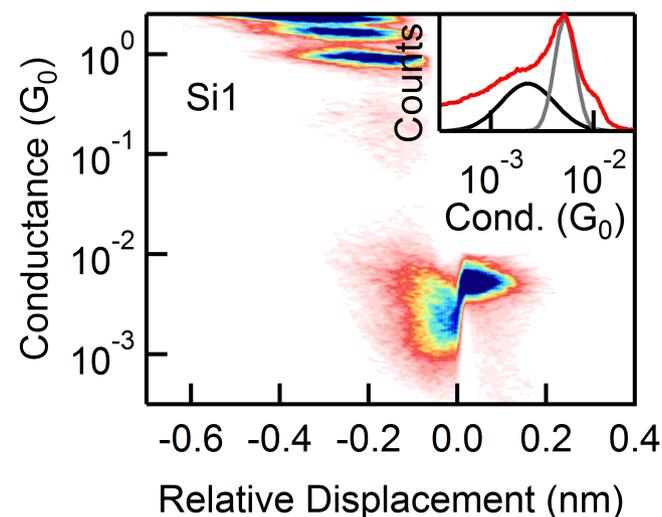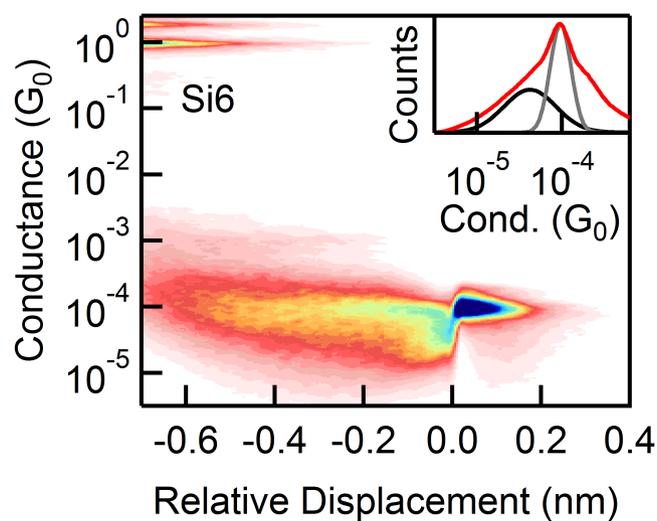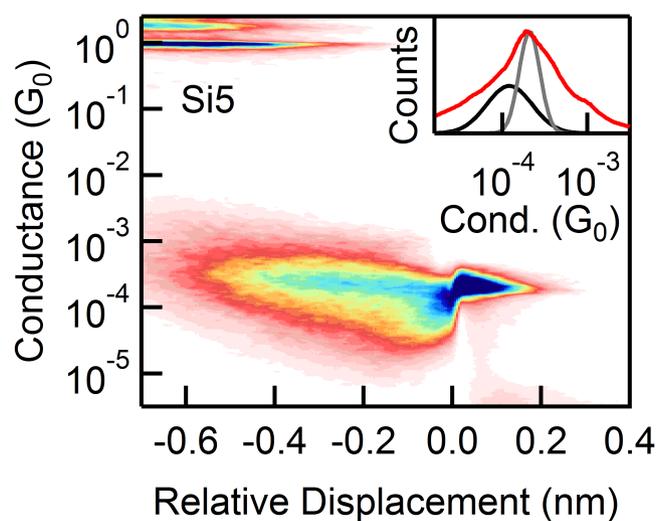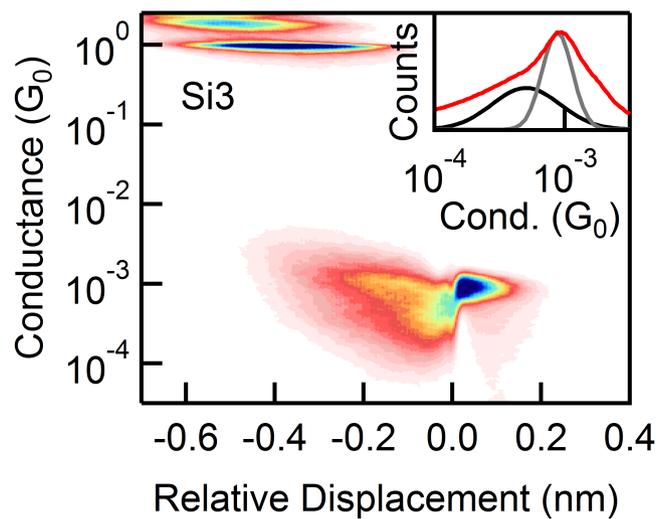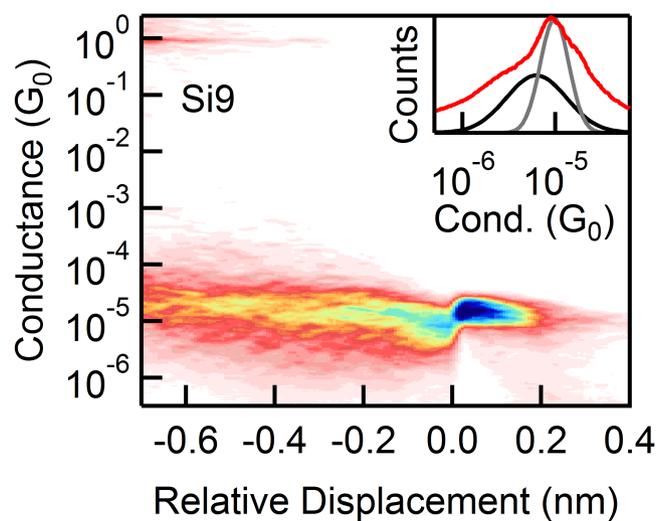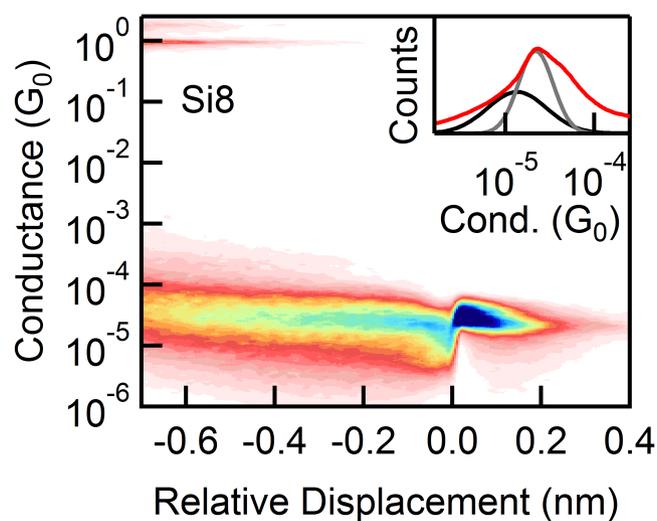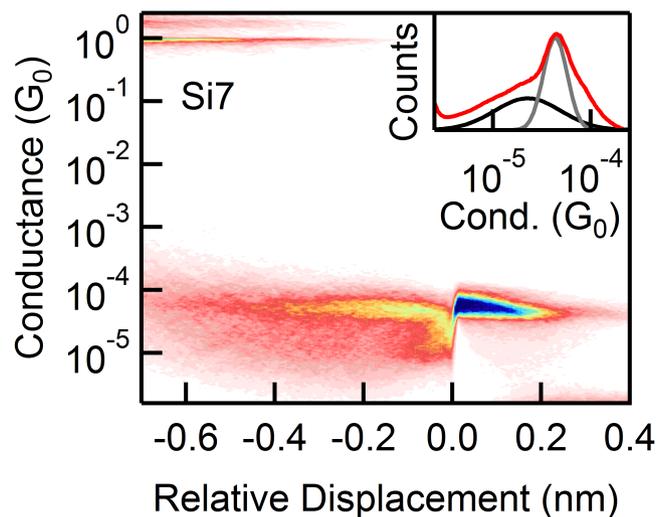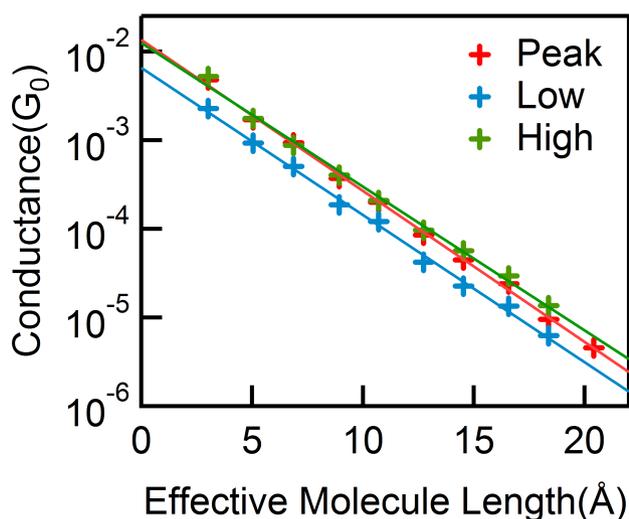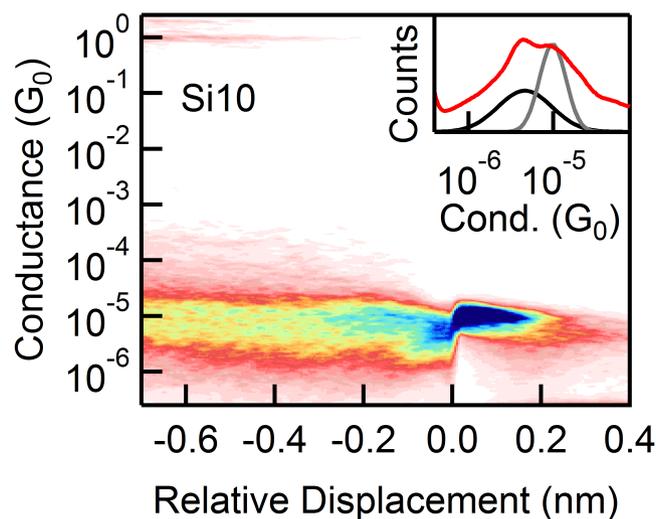
**Figure S2**: Here we compare the β values of the low G and high G peaks from the 1D histograms in the inset of Figure S1. "Peak" describes the value we get from the 1D histograms in Figure 3a without selection. The β values are as follows: Peak = 0.39 ± 0.01; High = 0.37 ± 0.01; Low = 0.38 ± 0.01. As described in the caption of Figure S1, the same analysis does not apply for **Si10**. The "contact resistance" of the high G state is 1.036 MΩ and 1.972 MΩ for the low G state.
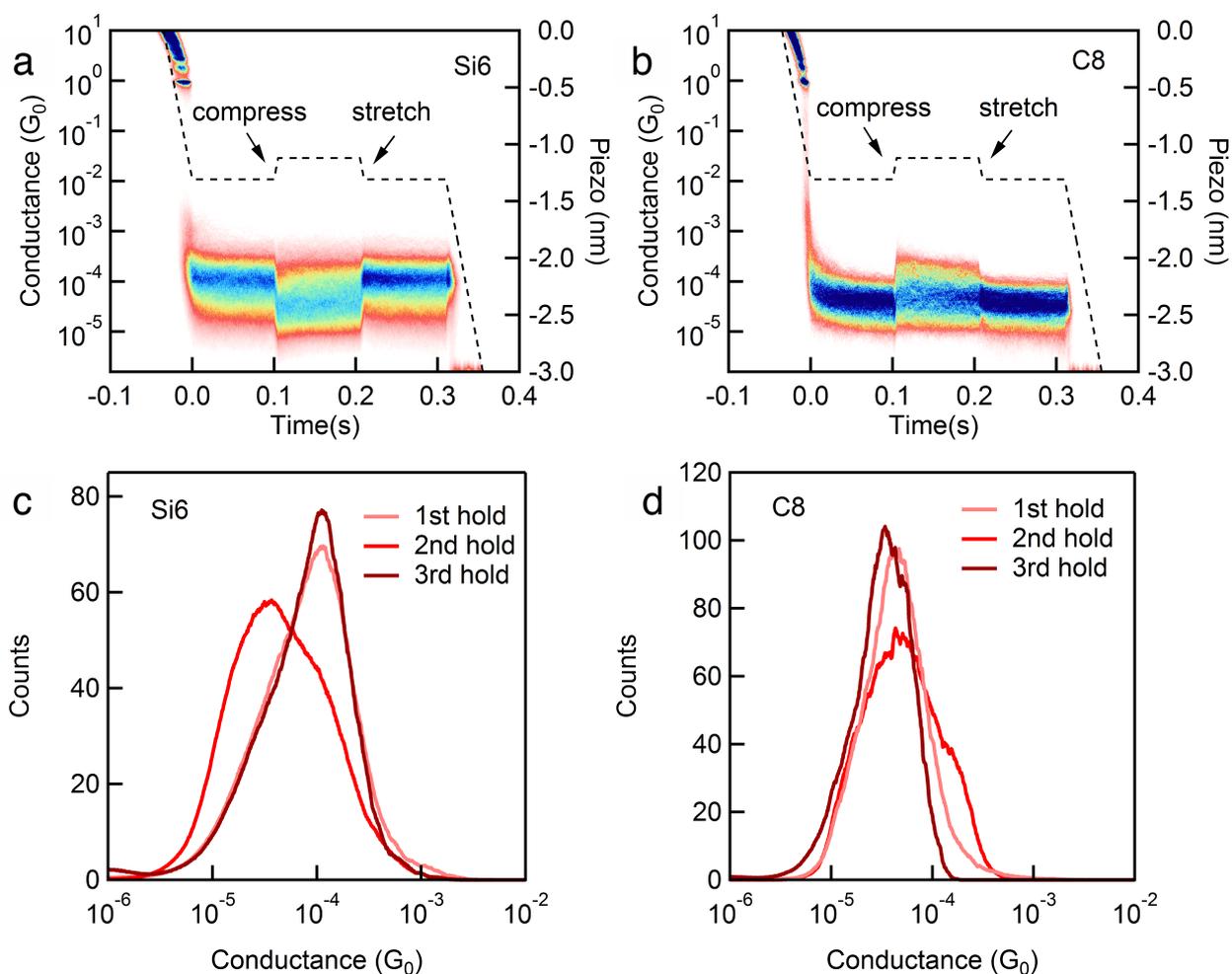
**Figure S3:** 2D histogram of compression-elongation experiment for **Si6** and **C8**. The histograms are constructed from all traces where a molecule remains in the junction during all three hold periods. No other selection is applied. We elongate the molecular junction, hold the junction in place for 0.1 s, compress the electrodes by 1.9 Å, hold the junction at this new displacement for another 0.1 s, then retract the electrodes until the junction breaks. (a) 2D histogram for **Si6** demonstrates switching between states over three hold periods. (b) 2D histogram for **C8** does not demonstrate switching between discrete states. (c) 1D histograms of the three hold periods for **Si6**. We observe some residual high G character in the 2$^{nd}$ hold period possibly from junctions that do not switch. (d) 1D histograms of the three hold periods for **C8**. We see that the peak maximum stays at approximately the same conductance during each hold period. The higher conducting shoulder in the 2$^{nd}$ hold period originates from the distance-dependent nature of tunneling.[1–5]
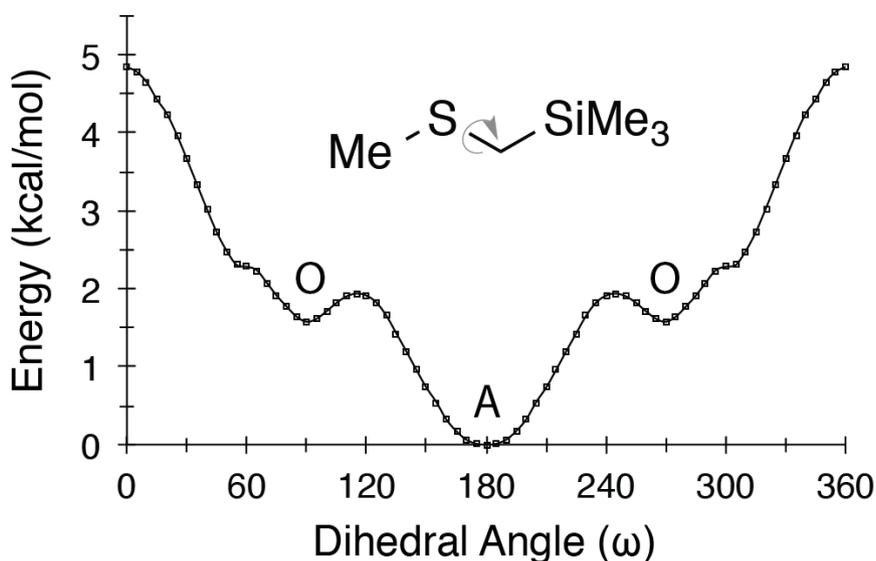
**Figure S4**: Energy plot for tetramethylsilylmethylsulfide $H_3C$-S-$CH_2$-$SiMe_3$. We find a global minimum (A) at $\omega=180°$ and two local minima (O) at $\omega=90°$ and $270°$. These geometries were calculated in 5˚ increments at the B3LYP/6-31G** level.
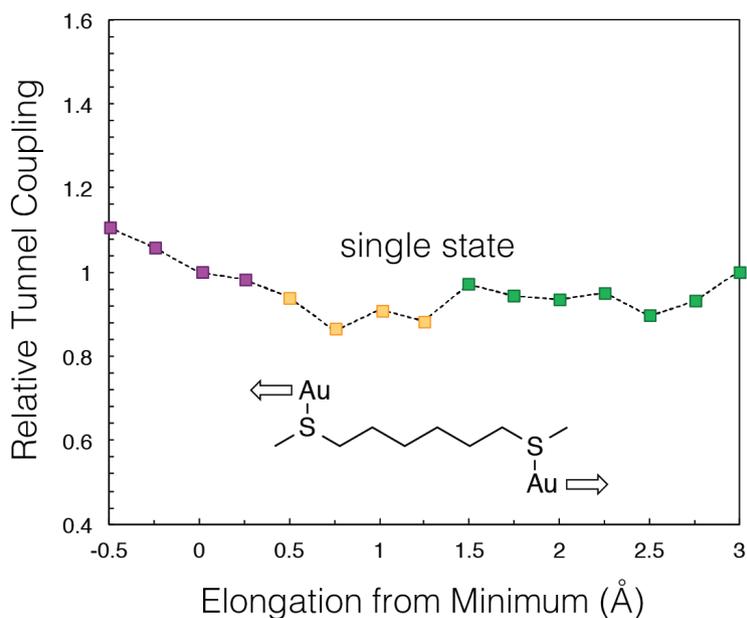


**Figure S5:** Tunnel coupling as a function of Au-Au distance plotted relative to the Elongation=0 point for the Au-**C6**-Au model system. The dihedral configurations are labeled with the same conventions from Figure 4 (A-A=purple, O-A=yellow, O-O=green).

## II. Detailed Analysis from Main Text

### i. The Different β Value for Oligosilanes with Thioanisole Linkers

In our previous study of the length-dependent properties in oligosilanes with thioanisole linkers[6], we found β = 0.27 Å$^{-1}$ for $n$=1-4. The longer oligomers with thioanisole contacts do not fall on the same fit and instead we find that $n$=4-6 fit to β = 0.46 Å$^{-1}$ (Figure S6 below). The high 'contact resistance' of the thioanisole linker prevented us from measuring oligomers longer than $n$=7. A rigorous study comparing the shorter and longer thioanisole-terminated oligosilanes is outside the scope of this manuscript; however, we offer here a simple qualitative reason for why they are different. For the short oligosilanes, the tunneling orbital is predominately comprised of the S pπ lone pair and aryl C π-orbitals so the tunneling orbital has much more π-character rather than σ-character. In the methylthiomethyl-terminated oligosilanes here, there are only σ-bonds between the two S atoms, so we never see a sudden change in our β plot where the σ-orbitals start to play a more dominant role as we do with the thioanisole-terminated silanes.
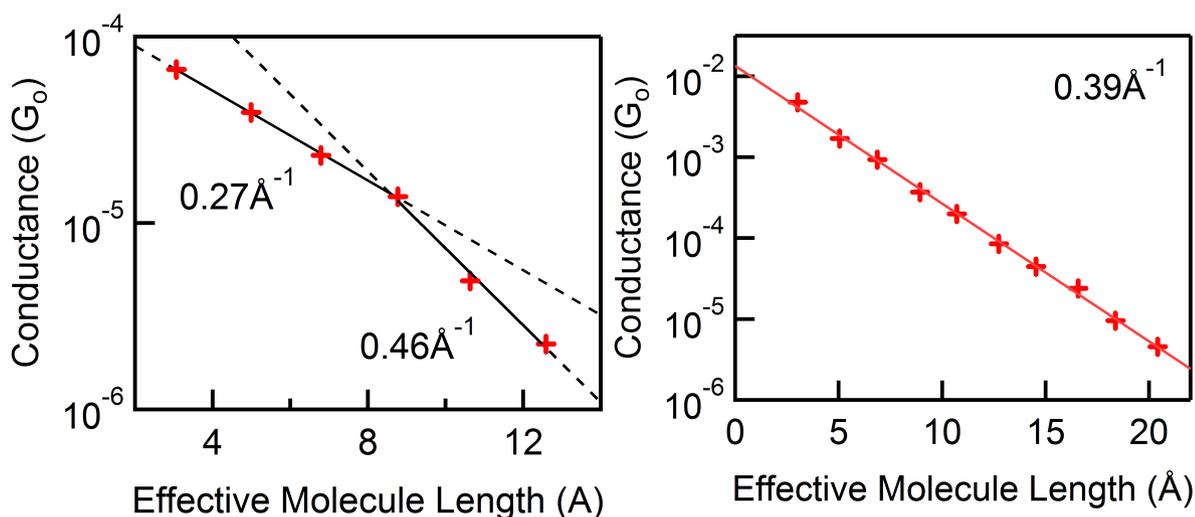


**Figure S6**: β plot for oligosilanes with thioanisole linkers (left) and methylthiomethyl linkers (right).

## ii. Rotations of the Internal Si-Si-Si-Si Dihedrals

We believe the geometry of the internal silane dihedral angles has a strong impact on conductance and that strong conjugation in the silane chain couples the stereoelectronics of the two terminal dihedrals. However, the consistent factor of 2 switching ratio and ~2 Å high G displacement length provide experimental evidence that rotation of the internal Si-Si-Si-Si dihedral angles does not account for the switching observed here. If the internal dihedral angles were responsible for switching, we would expect the high G displacement length to increase with the oligomer order (*n*) and for the switching ratio to increase with *n* as well. In other words, we would expect **Si4** and **Si9** to demonstrate markedly different switching behavior. Our experimental data shows that they do not.

In our calculations, we find that upon compression as well as elongation, the internal silane backbone angle remains relatively constant in a *transoid* form in the lowest energy geometries (Figure S7 below) while the terminal dihedral angles change significantly upon elongation. Michl *et al.*[7,8] have demonstrated that permethyloligosilanes, in contrast with the hydrogenated oligosilanes studied by George *et al.*,[9] settle into *transoid* ($\omega$=160-175°)[10] minima due to steric effects from the methyl groups.
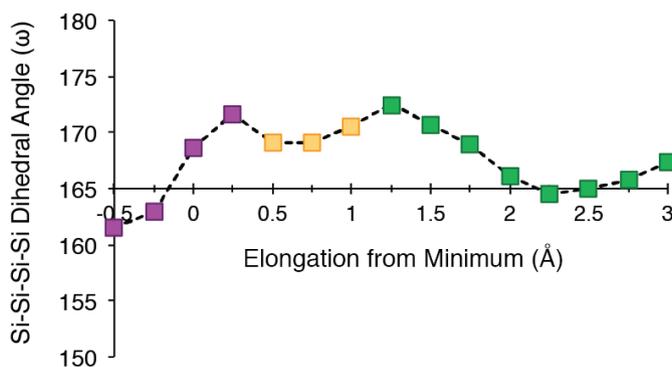


**Figure S7**: Si-Si-Si-Si dihedral angles for the lowest energy structures from Figure 4c (purple = A-A; yellow = O-A; green = O-O). Each lowest energy geometry at every Au-Au distance calculated has a *transoid* Si-Si-Si-Si geometry.

## III. General Synthetic Information

All reactions were performed in oven-dried or flame-dried round bottom flasks, unless otherwise noted. The flasks were fitted with rubber septa and reactions were conducted under a positive pressure of nitrogen or argon, unless otherwise noted. Anhydrous and anaerobic solvents were obtained from a Schlenk manifold with purification columns packed with activated alumina and supported copper catalyst (Glass Contour, Irvine, CA). Automated flash chromatography was performed using a Teledyne Isco Combiflash $R_f$200 and Redisep $R_f$ Gold Silica columns.

*Materials*. Commercial reagents were used without further purification. All reagents were purchased from Sigma-Aldrich, with the following exceptions. Chlorodimethylphenylsilane was purchased from Oakwood, Trifluoromethanesulfonic acid and dibromomethane were purchased from VWR, lithium bromide was purchased from Strem. The triethylamine hydrochloride was recrystallized from ethanol, collected, dried under high vacuum overnight, and stored in a desiccator.

*Instrumentation*. $^1$H, $^{13}$C, and $^{29}$Si NMR spectra were recorded on a Bruker DRX300 (300 MHz), Bruker DRX400 (400 MHz) or a Bruker DMX500 (500 MHz) spectrometer. Chemical shifts for protons are reported in parts per million downfield from tetramethylsilane and are referenced to residual protium in the NMR solvent (CHCl$_3$: δ 7.26; C$_6$H$_6$ δ 7.15). Chemical shifts for carbon are reported in parts per million downfield from tetramethylsilane and are referenced to the carbon resonances of the solvent (CDCl$_3$ δ 77.0; C$_6$D$_6$ δ 128.5). Chemical shifts for silicon are reported in parts per million downfield from tetramethylsilane and referenced to the silicon resonance of tetramethylsilane (TMS δ 0.0). Data are represented as follows: chemical shift, multiplicity (s = singlet, d = doublet, dd= doublet of doublets, t = triplet, m = multiplet), coupling constants in Hertz, and integration. The mass spectroscopic data were obtained at the Columbia

University mass spectrometry facility using a JEOL JMSHX110A/110A tandem mass spectrometer and Johns Hopkins University using a MASPEC II system [II32/1240].

## IV. Synthetic Procedures and Characterization of Compounds

$$Ph-Si-Cl \xrightarrow[\substack{\text{2. iPrMgCl, 0°C} \\ \text{3. Cl(SiMe}_2)_n\text{Cl, THF, 0°C}}]{\text{1. Li(0), THF, 0°C}} \left[ Ph-Si-Ph \right]_{n+2}$$
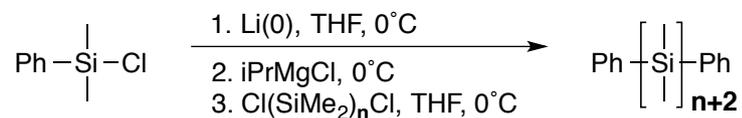
**i.** *α,ω-diphenylpermethyloligosilane 2 (n=3-10)*

α,ω-diphenylpermethyloligosilanes n=3-10 were synthesized from the same method. This reaction was performed under argon instead of nitrogen to prevent lithium nitride formation. Dichlorodimethylsilane and dichlorotetramethyldisilane were purchased from Aldrich; α,ω-dichloropermethyloligosilanes n=3-8 were synthesized as described below. Lithium granules (8.10 equiv.) were added to a 2-neck round bottom flask equipped with a stir bar. This flask was evacuated and cycled with argon 3x. THF was added to this flask (1 M with respect to the chlorodimethylphenylsilane). The flask was subsequently cooled to 0°C. The chlorodimethylphenylsilane (2.05 equiv.) was slowly added by syringe. After five minutes we observed red wisps coming off the lithium granules, indicative of silyl lithiate generation. This reaction mixture was allowed to warm to room temperature overnight and turned a deep red color. Under positive argon pressure, a coarse Schlenk filter stick capped with a Schlenk flask was fitted onto the 2-neck round bottom flask. This apparatus was inverted and the mixture was vacuum filtered. The 2-neck round-bottom was rinsed 2x with THF to wash the silyl lithiate off the remaining lithium granules. The Schlenk stick and 2-neck round bottom flask were removed and the Schlenk flask containing the silyl lithiate was capped with a septum. This flask was cooled to 0°C and a 2.0 M THF solution of isopropylmagnesium chloride (2.05 equiv.) was added via syringe. The reaction mixture was stirred at 0°C for 15 minutes and room temperature

for 15 minutes. The reaction was then cooled back down to 0°C and the α,ω-dichloropermethyloligosilane (1.00 equiv.) was added in a 1 M THF solution. This reaction was warmed to room temperature and stirred overnight. The excess Grignard was quenched with water (1 mL per 1 mmol of dichlorooligosilane) dropwise from a separatory funnel. A saturated ammonium chloride solution (1 mL per 2 mmol of dichlorooligosilane) was added dropwise from the same separatory funnel. The organic and aqueous layers were separated, and the aqueous layer was extracted with diethyl ether 3x. The organic layers were combined, washed with brine, dried with $MgSO_4$, filtered, and concentrated. The crude product was carried forward without further purification when the subsequent dichloropermethyloligosilane in the next step could be purified by distillation. When the subsequent dichloropermethyloligosilane could not be purified by distillation, the α,ω-diphenylpermethyloligosilane was purified by automated column chromatography on silica gel (100% hexanes).

*n=3:* Yellow oil (21.50 g). Carried forward without purification. The ^{1}H, ^{13}C, [29]Si, and HRMS match the characterization previously reported.[6]

*n=4:* Pale yellow semisolid (18.86 g). Carried forward without purification. The ^{1}H, ^{13}C, [29]Si, and HRMS match the characterization previously reported.[6].

*n=5:* White solid (9.38 g, 77% yield), purified by column chromatography. The ^{1}H, ^{13}C, [29]Si, and HRMS match the characterization previously reported.[6]

*n=6:* White solid (6.14 g, 68% yield), purified by column chromatography. ^{1}H NMR (500 MHz, $CDCl_3$) δ 7.47 - 7.40 (m, 4H), 7.35 - 7.29 (m, 6H), 0.37 (s, 12H), 0.10 (s, 12H), 0.04 (s, 12H). ^{13}C NMR (126 MHz, $CDCl_3$) δ 140.05, 133.89, 128.45, 127.84, -2.77, -4.34, -5.17. ^{29}Si NMR

(99 MHz, CDCl$_3$) δ -17.43, -38.51, -42.69. HRMS predicted for C$_{24}$H$_{46}$Si$_6$ 502.22, observed 502.2209 (FAB+).

*n=7:* White solid (3.26 g, 60% yield), purified by column chromatography. ^{1}H NMR (500 MHz, C$_6$D$_6$) δ 7.54 - 7.42 (m, 4H), 7.28 - 7.18 (m, 6H), 0.42 (s, 12H), 0.23 (s, 12H), 0.23 (s, 6H), 0.20 (s, 12H). ^{13}C NMR (126 MHz, C$_6$D$_6$) δ 139.91, 134.15, 128.83, 128.18, -2.69, -3.83, -4.05, -4.95. ^{29}Si NMR (60 MHz, CDCl$_3$) δ -17.70, -37.47, -38.53, -42.70. HRMS predicted for C$_{26}$H$_{52}$Si$_7$ 560.25, observed 560.2472 (FAB+).

*n=8:* White solid (3.37 g, 61% yield), purified by column chromatography. ^{1}H NMR (500 MHz, CDCl$_3$) δ 7.48 - 7.42 (m, 4H), 7.38 - 7.29 (m, 6H), 0.38 (s, 12H), 0.12 (s, 12H), 0.12 (s, 12H), 0.07 (s, 12H). ^{13}C NMR (126 MHz, CDCl$_3$) δ 140.06, 133.89, 128.46, 127.84, -2.76, -3.98, -4.23, -5.13. ^{29}Si NMR (99 MHz, CDCl$_3$) δ -17.93, -37.79, -38.90, -43.14. HRMS predicted for C$_{28}$H$_{58}$Si$_8$ 618.27, observed 618.2717 (FAB+).

*n=9:* White solid (1.75 g, 84% yield), purified by column chromatography. ^{1}H NMR (500 MHz, CDCl$_3$) δ 7.47 - 7.41 (m, 4H), 7.36 - 7.29 (m, 6H), 0.39 (s, 12H), 0.15 (s, 6H), 0.14 (s, 12H), 0.12 (s, 12H), 0.08 (s, 12H). ^{13}C NMR (126 MHz, CDCl$_3$) δ 140.06, 133.89, 128.46, 127.85, -2.75, -3.90, -3.93, -4.22, -5.12. ^{29}Si NMR (99 MHz, CDCl$_3$) δ -17.92, -37.68, -37.71, -38.87, -43.13. HRMS predicted for C$_{30}$H$_{64}$Si$_9$ 676.29, observed 676.2914 (FAB+).

*n=10:* White solid (1.39 g, 84% yield), purified by column chromatography. ^{1}H NMR (500 MHz, CDCl$_3$) δ 7.48 - 7.41 (m, 4H), 7.37 - 7.29 (m, 6H), 0.39 (s, 12H), 0.17 (s, 12H), 0.15 (s, 12H), 0.13 (s, 12H), 0.09 (s, 12H). ^{13}C NMR (126 MHz, CDCl$_3$) δ 140.07, 133.90, 128.46, 127.85, -2.75, -3.86, -3.92, -4.21, -5.11. ^{29}Si NMR (99 MHz, CDCl$_3$) δ -17.92, -37.62, -37.68, -38.85, -43.12. HRMS predicted for C$_{32}$H$_{70}$Si$_{10}$ 734.32, observed 735.3242 (FAB+).

**ii. α,ω-dichloropermethyloligosilane 3 (n=3-10)**
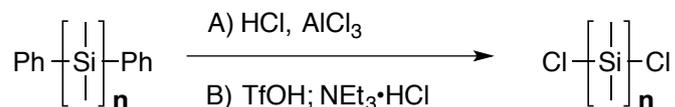


The α,ω-dichloropermethyloligosilanes were prepared by two methods.

Method A:

Anhydrous gaseous hydrogen chloride was generated from the careful addition of concentrated hydrochloric acid (15 mL, 37%) from an addition funnel to concentrated sulfuric acid (23 mL, 98%). Vigorous stirring of the concentrated sulfuric acid is essential to ensure adequate mixing (inadequate mixing results in a layer of HCl(aq) forming on top on H2SO4, which will react violently and explosively when disturbed). Caution should be used as both sulfuric acid and hydrochloric acid are toxic and corrosive. A glass pipette was pierced through a rubber septum to bubble the anhydrous HCl gas through the reaction mixture. The 2-neck round bottom was equipped with an adapter capped with inert tubing leading to a Dreschel bottle. Additional tubing from the Dreschel bottle outlet was submerged in saturated aqueous NaHCO3 to quench the excess HCl gas generated.

An oven-dried 2-neck round bottom flask equipped with a stir bar was charged with the α,ω-dichloropermethyloligosilane (1.00 equiv.) and the liquid was dissolved in anhydrous toluene (0.5 M). Aluminum chloride (0.06 equiv.) was added directly to the flask. Anhydrous hydrogen chloride was bubbled through the reaction at room temperature. The reaction was accompanied by a significant exotherm. After an hour, an aliquot was removed and conversion analyzed by 1H NMR spectroscopy in deuterated benzene. The aryl region was particularly informative of the reaction progress. The reaction continued until neither starting material nor

mono-protiodesilylated product was observed (3 hours). Over the course of the reaction, the mixture turned a deep orange color. The reaction mixture was sparged with argon for 15 minutes to drive off the HCl in solution. The reaction mixture was concentrated and hexanes was added to precipitate the aluminum chloride. The solution was then filtered over Celite through a Schlenk filter into a Schlenk flask. The hexane was removed under vacuum and the light yellow oily residue was distilled with a short path distillation head to yield a clear oil product. The moisture-sensitive dichloropermethyloligosilanes were stored in a glovebox.

Method B:

An oven-dried Schlenk flask equipped with a stir bar was charged with α,ω-dichloropermethyloligosilane (1.00 equiv.) and the liquid was dissolved in anhydrous dichloromethane (0.1 M with respect to dichlorosilane). This flask was cooled to 0°C and trifluoromethanesulfonic acid (2.03 equiv.) was added to the reaction flask via syringe (we advise the use of glass syringes because trifluoromethanesulfonic acid can erode plastic syringes quickly). This reaction mixture was stirred at 0°C for 30 minutes, then at room temperature for an hour. The dichloromethane was removed *in vacuo* to yield either an off-white oil or solid. The silyl triflate was reconstituted in diethyl ether (0.1 M) and cooled to 0°C. Triethylamine hydrochloride (2.03 equiv.) was added under a heavy flow of nitrogen. The reaction mixture was stirred at 0°C for 30 minutes, then room temperature for an hour. Over this period, a biphasic mixture formed due to the formation of the NEt$_3$•TfOH ionic liquid. This phase was typically pink-brown in color. The reaction flask was then cooled to -78°C to solidify the NEt$_3$•TfOH. The ether solution was then cannulated into a Schlenk flask. The ether was removed under vacuum and the remaining dichlorosilane was brought into the glovebox. These dichlorosilanes were

typically pure enough to proceed to the next reaction without further purification. The moisture-sensitive dichloropermethyloligosilanes were stored in a glovebox.

*n=3:* Clear, colorless oil (9.02 g, 64% yield). Synthesized from Method A, distilled at 45°C, 0.05 torr. $^1$H NMR (500 MHz, $C_6D_6$) δ 0.40 (s, 12H), 0.16 (s, 6H). $^{13}$C NMR (126 MHz, $C_6D_6$) δ 2.98, -7.65. $^{29}$Si NMR (60 MHz, $C_6D_6$) δ 25.42, -43.62.

*n=4:* Clear, colorless oil (8.13 g, 69% yield). Synthesized from Method A, distilled at 75°C, 0.05 torr. $^1$H NMR (500 MHz, $C_6D_6$) δ 0.40 (s, 12H), 0.21 (s, 12H). $^{13}$C NMR (126 MHz, $C_6D_6$) δ 3.26, -6.22. $^{29}$Si NMR (60 MHz, $C_6D_6$) δ 26.77, -42.51.

*n=5:* Clear, colorless oil (5.25 g, 77% yield). Synthesized from Method B, distilled at 100°C, 0.05 torr. $^1$H NMR (300 MHz, $C_6D_6$) δ 0.42 (s, 12H), 0.26 (s, 6H), 0.22 (s, 12H). $^{13}$C NMR (75 MHz, $C_6D_6$) δ 3.39, -4.70, -5.81. $^{29}$Si NMR (60 MHz, $C_6D_6$) δ 26.95, -40.93, -41.52.

*n=6:* White semisolid (5.12 g). Synthesized from Method B, carried forward without further purification. $^1$H NMR (500 MHz, $C_6D_6$) δ 0.44 (s, 12H), 0.27 (s, 12H), 0.24 (s, 12H). $^{13}$C NMR (126 MHz, $C_6D_6$) δ 3.40, -4.34, -5.74. $^{29}$Si NMR (60 MHz, $C_6D_6$) δ 29.66, -37.14, -38.23.

*n=7:* White solid (2.78 g). Synthesized from Method B, carried forward without further purification. $^1$H NMR (300 MHz, $C_6D_6$) δ 0.45 (s, 12H), 0.28 (s, 12H), 0.27 (s, 6H), 0.26 (s, 12H). $^{13}$C NMR (75 MHz, $C_6D_6$) δ 3.44, -3.95, -4.22, -5.67. $^{29}$Si NMR (60 MHz, $C_6D_6$) δ 27.23, -37.75, -39.50, -40.71.

*n=8:* White solid (3.08 g). Synthesized from Method B, carried forward without further purification. Z$^1$H NMR (500 MHz, $C_6D_6$) δ 0.46 (s, 12H), 0.30 (s, 12H), 0.29 (s, 12H), 0.27 (s, 12H). $^{13}$C NMR (126 MHz, $C_6D_6$) δ 3.45, -3.84, -4.17, -5.64. $^{29}$Si NMR (99 MHz, $C_6D_6$) δ 27.28, -37.53, -39.40, -40.66.

_n=9:_ White solid (1.62 g). Synthesized from Method B, carried forward without further purification. ^{1}H NMR (500 MHz, $C_6D_6$) δ 0.47 (s, 12H), 0.32 (s, 12H), 0.31 (two overlapping singlets, 18H), 0.28 (s, 12H). ^{13}C NMR (126 MHz, $C_6D_6$) δ 3.46, -3.73, -3.78, -4.14, -5.62. ^{29}Si NMR (99 MHz, $C_6D_6$) δ 27.29, -37.31, -37.43, -39.36, -40.64.

_n=10:_ White solid (1.05 g). Synthesized from Method B, carried forward without further purification. ^{1}H NMR (500 MHz, $C_6D_6$) δ 0.47 (s, 12H), 0.35 - 0.27 (overlapping singlets, 48H). ^{13}C NMR (126 MHz, $C_6D_6$) δ 3.47, -3.67, -3.75, -4.12, -5.62. ^{29}Si NMR (99 MHz, $C_6D_6$) δ 27.31, -37.22, -37.39, -39.35, -40.63.

**iii.** _α,ω-bis(bromomethyl)oligosilane **4** (n=1-2)_
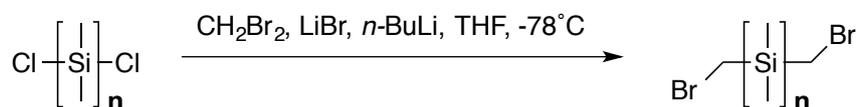


An oven-dried round bottom flask equipped with a stir bar and septum was brought into the glovebox. Anhydrous lithium bromide (2.00 equiv.) was added to this flask. THF was added to the flask (0.143 M with respect to the dichlorooligosilane), followed by the dichlorooligosilane (1.00 equiv.) and dibromomethane (4.00 equiv.). A slight yellow coloration was observed upon mixing these constituents. The reaction flask was cooled to -78°C and submerged deeply into the dry ice-acetone bath to ensure the sides of the glass were cold as well. A 1.64 M solution of _n_-butyllithium in hexanes (3.00 equiv.) was added to the reaction flask very slowly down the side of the flask using a syringe pump. We achieved low yields when adding the butyllithium too quickly; a slow generation of the bromomethyl lithate is desirable. The butyllithium was added in this fashion over an hour. The reaction mixture was warmed slowly to room temperature overnight. The THF was evaporated and the remaining residue was stirred

with hexanes for 5 minutes. After this period, the hexanes solution was filtered over Celite and evaporated to yield a crude oil product. This material was then chromatographed over silica in 100% hexanes and visualized with Hanessian's Stain to achieve the desired product. We note that our mass spectrometry facility was unable to ionize the α,ω-bis(bromomethyl)oligosilanes so mass spectrometry analysis for these intermediate compounds is not provided.

<u>n=1:</u> Clear, colorless oil (0.79 g, 45% yield). $^1$H NMR (300 MHz, CDCl$_3$) δ 2.58 (s, 4H), 0.29 (s, 6H). $^{13}$C NMR (126 MHz, CDCl$_3$) δ 15.03, -4.56. $^{29}$Si NMR (60 MHz, CDCl$_3$) δ 3.37.

<u>n=2:</u> Clear, colorless oil (1.04 g, 69% yield). $^1$H NMR (300 MHz, CDCl$_3$) δ 2.63 (s, 4H), 0.25 (s, 12H). $^{13}$C NMR (126 MHz, CDCl$_3$) δ 17.65, -3.71. $^{29}$Si NMR (60 MHz, CDCl$_3$) δ -14.07.

*α,ω-bis(chloromethyl)permethyloligosilane **4** (n=3-10)*
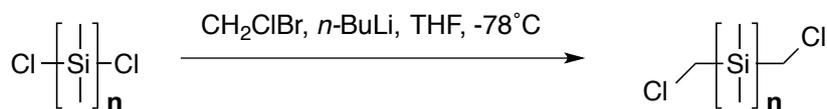


We synthesized the *n*=3-10 oligomers from bromochloromethane that pre-existed in our laboratory. However, we note that at the time of this publication chloroiodomethane is commercially available while bromochloromethane is not. Others have shown that both chloro-iodomethane and bromochloromethane are effective in installing chloromethyl endgroups. [11]

The α,ω-bis(chloromethyl)permethyloligosilanes were synthesized from a method adapted from Kobayashi and Pannell.[12] A flame-dried round bottom flask equipped with a stir bar and septum was charged with the α,ω-dichloropermethyloligosilane **3** (1.00 equiv.) followed by the bromochloromethane (3.00 equiv.) and THF as solvent. Due to the poor solubility of the

higher oligosilanes, especially at lower temperatures, we found that higher yields were obtained under dilute conditions (0.03 M) relative to more concentrated conditions (0.18 M). The $n$=8-10 oligosilanes were synthesized under dilute conditions for this reason to improve yield. The reaction flask was cooled to -78˚C and submerged deeply into the dry ice-acetone bath to ensure the sides of the glass were cold. A 1.64 M solution of $n$-butyllithium in hexanes (2.03 equiv.) was added to the reaction flask very slowly down the side of the flask using a syringe pump over an hour. The reaction mixture was warmed slowly to room temperature overnight. The THF was evaporated and the remaining residue was stirred with hexanes for 5 minutes, after which it was filtered over an alumina plug and evaporated. In most instances, this material was pure enough to carry forward without further purification. Our mass spectrometry facility was unable to ionize the α,ω-bis(chloromethyl)permethyloligosilanes so mass spectrometry analysis for these compounds is not provided.

_n=3:_ Clear, colorless oil (1.40 g, 93% yield). ^{1}H NMR (500 MHz, CDCl$_3$) δ 2.92 (s, 4H), 0.22 (s, 12H), 0.20 (s, 6H). ^{13}C NMR (126 MHz, CDCl$_3$) δ 31.47, -4.19, -6.27. ^{29}Si NMR (60 MHz, CDCl$_3$) δ -11.07, -48.86.

_n=4:_ Clear, colorless oil (1.56 g, 91% yield). ^{1}H NMR (400 MHz, CDCl$_3$) δ 2.91 (s, 4H), 0.21 (s, 12H), 0.20 (s, 12H). ^{13}C NMR (126 MHz, CDCl$_3$) δ 31.66, -3.99, -5.41. ^{29}Si NMR (60 MHz, CDCl$_3$) δ -10.60, -44.77.

_n=5:_ Clear, colorless oil (0.58 g). This material had significant impurities in the NMR, but was carried forward anyway and purified in the next step.

_n=6:_ Clear, colorless oil (0.37 g, 83% yield). ^{1}H NMR (500 MHz, CDCl$_3$) δ 2.92 (s, 4H), 0.22 - 0.20 (three overlapping singlets, 36H). ^{13}C NMR (126 MHz, CDCl$_3$) δ 31.82, -3.98, -4.19, -5.11.

$^{29}$Si NMR (60 MHz, CDCl$_3$) δ -10.67, -39.36, -43.30.

_n=7:_ White, waxy solid (0.34 g, 71% yield). $^1$H NMR (500 MHz, CDCl$_3$) δ 2.92 (s, 4H), 0.22 - 0.20 (four overlapping singlets, 42H). $^{13}$C NMR (126 MHz, CDCl$_3$) δ 31.86, -3.93, -3.99, -4.16, -5.10. $^{29}$Si NMR (99 MHz, CDCl$_3$) δ -10.68, -37.87, -39.30, -43.26.

_n=8:_ White, waxy solid (0.52 g, 60% yield). $^1$H NMR (500 MHz, CDCl$_3$) δ 2.92 (s, 4H), 0.22-0.20 (four overlapping singlets, 48H). $^{13}$C NMR (126 MHz, CDCl$_3$) δ 31.88, -3.89, -3.99, -4.13, -5.09. $^{29}$Si NMR (99 MHz, CDCl$_3$) δ -10.68, -37.77, -39.22, -43.25.

_n=9:_ White, waxy solid (431 mg, 55% yield). $^1$H NMR (500 MHz, CDCl$_3$) δ 2.92 (s, 4H), 0.22-0.20 (five overlapping singlets, 54H). $^{13}$C NMR (126 MHz, CDCl$_3$) δ 31.91, -3.84, -3.85, -3.98, -4.11, -5.08. $^{29}$Si NMR (99 MHz, CDCl$_3$) δ -10.68, -37.66, -37.69, -39.21, -43.25.

_n=10:_ White, waxy solid (295 mg, 48% yield). $^1$H NMR (300 MHz, CDCl$_3$) δ 2.92 (s, 4H), 0.22-0.20 (five overlapping singlets, 60H). $^{13}$C NMR (126 MHz, CDCl$_3$) δ 31.74, -3.97, -4.00, -4.14, -4.27, -5.24. $^{29}$Si NMR (99 MHz, CDCl$_3$) δ -10.68, -37.58, -37.66, -39.20, -43.24.

**iv.** *α,ω-bis(thiomethyl)permethyloligosilane Si1-Si10 (n=1-10)*
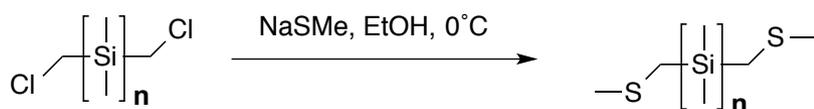


Sodium thiomethoxide (3.00 equiv.) was weighed out into a 20 mL scintillation vial equipped with a stir bar. Ethanol (0.1 M with respect to the α,ω-bis(chloromethyl)-permethyloligosilane) was added to the vial, and the vial was cooled to 0˚C. The α,ω-bis(chloromethyl)permethyloligosilane (1.00 equiv.) was added neat for *n*=1-6 or dissolved in THF (0.1 M) for *n*=7-10. The reaction was run for three hours or allowed to stir overnight. After

evaporating the solvent, the residue was redissolved in hexanes or dichloromethane and filtered over alumina (the longer oligosilanes ($n \geq 8$) are marginally soluble in hexanes). If the $^1$H NMR of the crude material was not clean, the crude residue was purified by silica gel chromatography.

_n=1:_ Clear, colorless oil (42 mg, 28% yield). Purified via alumina plug with hexanes. $^1$H NMR (500 MHz, CDCl$_3$) δ 2.17 (s, 6H), 1.88 (s, 4H), 0.19 (s, 6H). $^{13}$C NMR (126 MHz, CDCl$_3$) δ 20.50, 19.90, -3.27. $^{29}$Si NMR (60 MHz, CDCl$_3$) δ 1.02. HRMS predicted for C$_6$H$_{16}$S$_2$Si 180.05, observed 180.0460 (FAB+).

_n=2:_ Clear, colorless oil (152 mg, 78% yield). Purified via alumina plug with hexanes. $^1$H NMR (300 MHz, CDCl$_3$) δ 2.17 (s, 6H), 1.93 (s, 4H), 0.19 (s, 12H). $^{13}$C NMR (126 MHz, CDCl$_3$) δ 20.78, 20.51, -3.68. $^{29}$Si NMR (60 MHz, CDCl$_3$) δ -17.48. We attempted HRMS on this compound numerous times, but only observed the mass fragment corresponding to [H$_3$C-S-CH$_2$-SiMe$_2$-SiMe$_2$]$^+$. HRMS predicted for C$_6$H$_{17}$SSi$_2$ 177.06, observed 177.0590 (FAB+).

_n=3:_ Clear, colorless oil (81 mg, 37% yield). Purified by silica chromatography with a gradient from 100% hexanes to 70%/30% hexanes/dichloromethane. $^1$H NMR (300 MHz, CDCl$_3$) δ 2.16 (s, 6H), 1.92 (s, 4H), 0.19 (s, 12H), 0.18 (s, 6H). $^{13}$C NMR (126 MHz, CDCl$_3$) δ 21.04, 20.79, -3.12, -6.22. $^{29}$Si NMR (60 MHz, CDCl$_3$) δ -14.16, -48.05. HRMS predicted for C$_{10}$H$_{28}$S$_2$Si$_3$ 296.09, observed 295.0870 (FAB+).

_n=4:_ Clear, colorless oil (275 mg, 86% yield). Purified via alumina plug with hexanes. $^1$H NMR (500 MHz, CDCl$_3$) δ 2.16 (s, 6H), 1.91 (s, 4H), 0.19 (two overlapping singlets, 24H). $^{13}$C NMR (126 MHz, CDCl$_3$) δ 21.16, 20.79, -2.96, -5.35. $^{29}$Si NMR (60 MHz, CDCl$_3$) δ -13.52, -44.43. HRMS predicted for C$_{12}$H$_{34}$S$_2$Si$_4$ 354.12, observed 353.1100 (FAB+).

*n=5:* Clear, colorless oil (35 mg, 11% yield). Purified by silica gel chromatography with gradient from 100% hexanes to 7:3 hexanes: dichloromethane. $^1$H NMR (500 MHz, CDCl$_3$) δ 2.16 (s, 6H), 1.90 (s, 3H), 0.20 (s, 6H), 0.19 (two overlapping singlets, 24H). $^{13}$C NMR (126 MHz, CDCl$_3$) δ 21.16, 20.80, -2.95, -4.37, -5.14. $^{29}$Si NMR (60 MHz, CDCl$_3$) δ -13.53, -40.73, -43.07. HRMS predicted for C$_{14}$H$_{40}$S$_2$Si$_5$ 412.14, observed 412.1328 (FAB+).

*n=6:* Clear, colorless oil (76 mg, 40% yield). Purified by silica gel chromatography with gradient from 100% hexanes to 7:3 hexanes: dichloromethane. $^1$H NMR (500 MHz, CDCl$_3$) δ 2.16 (s, 6H), 1.90 (s, 4H), 0.21 (s, 12H), 0.19 (two overlapping singlets, 24H). $^{13}$C NMR (126 MHz, CDCl$_3$) δ 21.19, 20.80, -2.93, -4.13, -5.09. $^{29}$Si NMR (60 MHz, CDCl$_3$) δ -13.75, -39.56, -43.21. HRMS predicted for C$_{16}$H$_{46}$S$_2$Si$_6$ 470.17, observed 469.1593 (FAB+).

*n=7:* Clear, colorless oil (22 mg, 11% yield). Purified by silica gel chromatography with gradient from 100% hexanes to 7:3 hexanes: dichloromethane. $^1$H NMR (500 MHz, CDCl$_3$) δ 2.16 (s, 6H), 1.90 (s, 4H), 0.21 (two overlapping singlets, 18H), 0.19 (two overlapping singlets, 24H). $^{13}$C NMR (126 MHz, CDCl$_3$) δ 21.18, 20.80, -2.94, -3.91, -4.10, -5.08. $^{29}$Si NMR (99 MHz, CDCl$_3$) δ -13.51, -37.89, -39.22, -42.92. HRMS predicted for C$_{18}$H$_{52}$S$_2$Si$_7$ 528.19, observed 528.1940 (FAB+).

*n=8:* White semisolid (42 mg, 32% yield). Purified via alumina plug with hexanes to remove impurities, then dichloromethane to extract product. $^1$H NMR (500 MHz, CDCl$_3$) δ 2.16 (s, 6H), 1.90 (s, 4H), 0.21 (two overlapping singlets, 24H), 0.19 (two overlapping singlets, 24H). $^{13}$C NMR (126 MHz, CDCl$_3$) δ 21.18, 20.80, -2.94, -3.87, -4.08, -5.07. $^{29}$Si NMR (99 MHz, CDCl$_3$) δ -13.51, -37.77, -39.15, -42.90. HRMS predicted for C$_{20}$H$_{58}$S$_2$Si$_8$ 586.21, observed 586.2134 (FAB+).

*n=9:* White semisolid (73 mg, 34% yield). Purified via alumina plug with hexanes to remove impurities, then dichloromethane to extract product. ^{1}H NMR (500 MHz, CDCl$_3$) δ 2.17 (s, 6H), 1.91 (s, 4H), 0.21-0.19 (five overlapping singlets, 54H). ^{13}C NMR (126 MHz, CDCl$_3$) δ 21.14, 20.75, -2.93, -3.83, -3.85, -4.07, -5.07. ^{29}Si NMR (99 MHz, CDCl$_3$) δ -13.48, -37.66, -37.70, -39.08, -42.85. HRMS predicted for C$_{22}$H$_{64}$S$_2$Si$_9$ 644.24, observed 644.2402 (FAB+).

*n=10:* White semisolid (25 mg, 13% yield). Purified via alumina plug with hexanes to remove impurities, then dichloromethane to extract product. ^{1}H NMR (500 MHz, CDCl$_3$) δ 2.16 (s, 6H), 1.90 (s, 4H), 0.21-0.19 (six overlapping singlets, 60H). ^{13}C NMR (126 MHz, CDCl$_3$) δ 21.18, 20.80, -2.93, -3.81, -3.84, -4.07, -5.07. ^{29}Si NMR (99 MHz, CDCl$_3$) δ -13.50, -37.59, -37.68, -39.13, -42.89. HRMS predicted for C$_{24}$H$_{70}$S$_2$Si$_{10}$ 702.26, observed 701.2533 (FAB+).

## V. STM-Break Junction Experiments

### i. General Details

We measure the conductance of single molecules attached to gold electrodes using a home-built modified Scanning Tunneling Microscope (STM). We use a hand-cut 0.25 mm diameter gold wire (99.998%, Alfa Aesar) as the STM tip and a gold-coated (99.999%, Alfa Aesar) mica surface as the substrate. A commercially available single-axis piezoelectric positioner (Nano-P15, Mad City Labs) is used to achieve sub-angstrom level control of the tip-substrate distance. The STM is controlled using a custom written program in IgorPro (Wavemetrics, Inc.) and operates in ambient conditions at room temperature. The gold substrate is UV/Ozone cleaned for 15 minutes immediately before use. After we collect at least a thousand traces to ensure that the gold is clean, we introduce our molecules dissolved in 1,2,4-trichlorobenzene (Sigma-Aldrich or Alfa Aesar, 99% purity). The solvent concentrations for the oligosilanes were as follows: 1mM for **Si1-Si6**, 0.1mM for **Si7-Si9**, 0.05mM for **Si10**.

We move the tip in and out of the substrate to create a gold metal contact with a conductance of at least 5 $G_0$ before withdrawing the tip. We record the current as a function of tip/substrate displacement with an applied bias of 25 mV for **Si1-3**, 50 mV for **Si4**, 225 mV for **Si5-7**, 660 mV for **Si8-10**. The tip is withdrawn from the substrate at a speed of about 19 nm/s and the data is collected at a 40 kHz acquisition rate. For each molecule studied, we collect over 10,000 traces to create 1D conductance histograms (Figure 3a) without data selection.

## ii. Data analysis for 2D histograms

2D conductance histograms (Figure 3d in the manuscript and Supplementary Figure S1) were generated using the selection algorithm flow chart shown below.

```
                          Start
                            │
                            ▼
               Conductance breaks
                 cleanly to noise?
              No ↙              ↘ Yes
          Rejected        At least one sharp drop
                             in molecule step?
                          No ↙              ↘ Yes
                      Rejected        The last drop is a low-to-
                                          high switch?
                                      No ↙          ↘ Yes
                                   Rejected        Selected
```
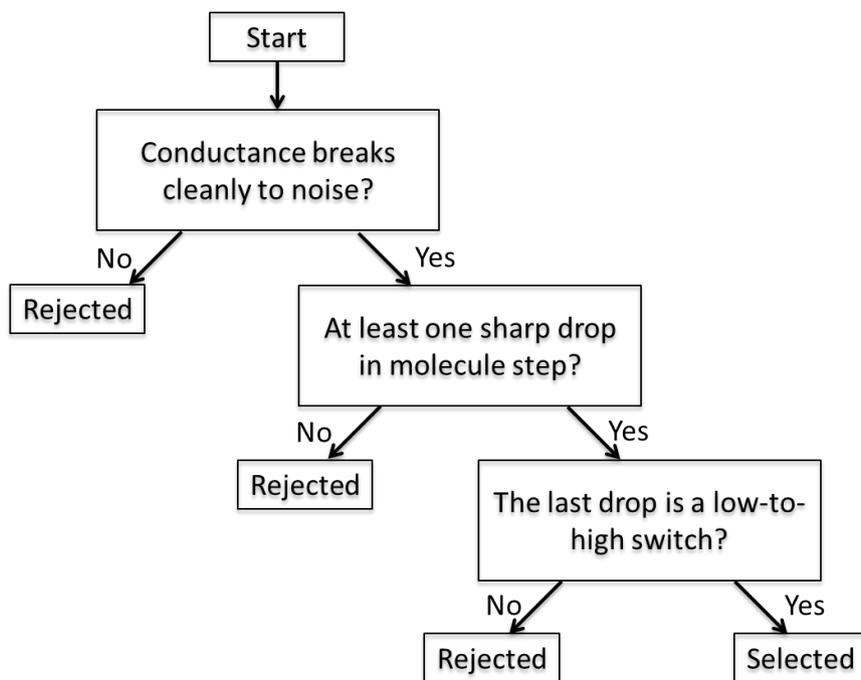
First, we select the traces that demonstrate a clean break in conductance from the molecular plateau to the noise level of the instrument ($3 \times 10^{-6}$ $G_0$). This ensures that we are selecting traces where a junction rupture event occurs. Second, we select traces that demonstrate at least one abrupt conductance change from within the plateau, which we define as a switching event. We use an algorithm that includes looking at the conductance derivative to identify such events following a procedure detailed in Aradhya et al.[13] as shown in Supplementary Figure S8. We scan this derivative plot from right to left and select the first maximum above an oligosilane-specific threshold (we determine this threshold from trace-by-trace analysis). This allows us to align the traces to the final switching event. Finally, we select traces that demonstrate a switch from low to high conductance. We use 100 data points on both sides of the drop to compare the

two conductance states. All traces are aligned to zero-displacement at their switch position to construct the 2D histogram. These three criteria ensure that selection is not based on conductance plateau value, plateau shape or plateau length.
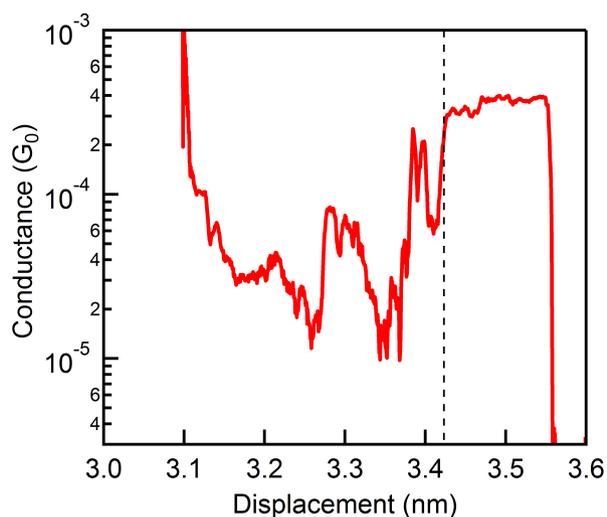


**Figure S8**: A sample trace of **Si4** showing the location of the switch as determined following our algorithm. The black dashed line denotes the switch position where we align the trace to zero-displacement in the 2D histogram.

### V. Computational Chemistry

### i. General Methods

Our experimental data demonstrates that conductance rises by a factor of two in the final ~2 Å of measurement for all oligosilanes due to some systematic change in molecular geometry induced from pulling the electrodes apart. In light of these experimental results, our principal interest in our computational model was to understand how the geometry of the molecule itself changes as the distance between the two Au atoms that participate in each terminal S-Au linkage increases. We therefore reasoned that our computational studies would reveal the same general molecular behavior regardless of whether we stretched the molecule between two single gold atoms or between two large slabs of many gold atoms. Based on this reasoning, we decided to study the simplest possible system: the Au-molecule-Au complex.

The calculated bond between the S $p\pi$ orbital and a neutral Au atom is very weak (2.70-2.75 Å) and is therefore a poor representation of the strong force of pulling by the electrodes that we see in our experiments. The interaction between the S $p\pi$ lone pair and $Au^+$ is significantly stronger (2.34-2.43 Å) and is also close to the calculated equilibrium bond length between a $Au_5$ cluster and S $p\pi$ orbital (2.45 Å).[15] We also reasoned that the positive character of the $Au^+$ cation might serve as a better mimic for the Lewis acidic nature of the undercoordinated Au contact atom. This indicated to us that the $Au^+$ cation was a suitable proxy for the gold electrode in our geometry optimizations. Our approach naturally results in an overestimation of the Au-S interaction. While we cannot compare the exact quantities that arise from these calculations to our experiment or to the calculations of others, we can compare the quantities within each specific computational system as depicted in Figures 4b, 4c, and S5. We can then compare the trends we observe within each computational system to the trends we observe in our experiment. In doing so, we use our model to demonstrate that the dihedral conformation of the molecule

shifts from A-A to O-A to O-O as mechanical strain increases, and that the O-O state is more conductive because the strong σ-conjugation in the silane enhances coupling between the Au atoms.

All DFT calculations were carried out with Jaguar (version 8.3, Schrodinger, LLC, New York, NY, 2014). We used a B3LYP functional for all molecules, a 6-31G** basis set for light atoms, and a LACVP** basis set for Au atoms.[14] We calculate the tunnel coupling for the **Si4** (Figure 4c) and **C6** (Figure S5) systems with the same method. We use the $Au^+$ cation to mimic the gold electrodes and provide us with reasonable molecular geometries for our tunnel coupling calculations on the neutral Au-molecule-Au complex. We shorten and elongate the distance between the Au atoms in 0.25 Å increments in the $[Au\text{-molecule-}Au]^{2+}$ complex while allowing the rest of the molecular geometry to fully relax. We take the lowest energy geometries that arise from these studies and perform single point energy calculations on their neutral (as opposed to doubly oxidized) form and take the resulting HOMO-LUMO energy splitting as the tunnel coupling quantity, 2t. We plot the square of the tunnel coupling ($4t^2$) against Au-Au distance to study how the interplay between electrode distance and molecular geometry affects electronic coupling through the molecule.

In Figure 4b we study how the relative energies between the three conformations change with Au-Au distance. In addition to constraining the Au-Au distance, we constrain the two terminal $Me\text{-}S\text{-}CH_2\text{-}SiMe_2\text{-}$ dihedral angles to ±174˚ for A-A, 174˚ and -93˚ for O-A, and ±93˚ for O-O (these values were found from preliminary calculations). We subtract the energy of the A-A configuration from the energies of the A-A, O-A, and O-O configurations that we find at each particular Au-Au distance. We plot our energies this way to ensure that the energies of the three conformations are only compared relative to each other at each specific Au-Au distance.

**Table ST1:** *Relative Energies for A-A, O-A, and O-O Configurations with Fixed Dihedrals for [Au-Si4-Au]$^{2+}$ (Figure 4b)*

| Dihedral Config. | | A-A | | O-A | | O-O | |
|---|---|---|---|---|---|---|---|
| Au-Au Distance (Å) | Elongation (Å) | Total Energy (Hartrees) | Rel. Energy (kcal/mol) | Total Energy (Hartrees) | Rel. Energy (kcal/mol) | Total Energy (Hartrees) | Rel. Energy (kcal/mol) |
| 13.25 | -0.50 | -2702.6576 | 0 | -2702.6570 | 0.42 | -2702.6562 | 0.90 |
| 13.50 | -0.25 | -2702.6585 | 0 | -2702.6577 | 0.51 | -2702.6546 | 2.45 |
| 13.75 | 0.00 | -2702.6590 | 0 | -2702.6583 | 0.45 | -2702.6553 | 2.34 |
| 14.00 | 0.25 | -2702.6589 | 0 | -2702.6587 | 0.12 | -2702.6559 | 1.87 |
| 14.25 | 0.50 | -2702.6582 | 0 | -2702.6590 | -0.49 | -2702.6564 | 1.13 |
| 14.50 | 0.75 | -2702.6573 | 0 | -2702.6590 | -1.08 | -2702.6571 | 0.12 |
| 14.75 | 1.00 | -2702.6560 | 0 | -2702.6586 | -1.64 | -2702.6579 | -1.15 |
| 15.00 | 1.25 | -2702.6541 | 0 | -2702.6577 | -2.25 | -2702.6585 | -2.74 |
| 15.25 | 1.50 | -2702.6512 | 0 | -2702.6564 | -3.28 | -2702.6591 | -4.98 |
| 15.50 | 1.75 | -2702.6477 | 0 | -2702.6548 | -4.46 | -2702.6595 | -7.41 |
| 15.75 | 2.00 | -2702.6432 | 0 | -2702.6522 | -5.62 | -2702.6590 | -9.89 |
| 16.00 | 2.25 | -2702.6378 | 0 | -2702.6490 | -7.02 | -2702.6578 | -12.54 |
| 16.25 | 2.50 | -2702.6318 | 0 | -2702.6444 | -7.93 | -2702.6554 | -14.83 |
| 16.50 | 2.75 | -2702.6251 | 0 | -2702.6385 | -8.41 | -2702.6521 | -16.95 |
| 16.75 | 3.00 | -2702.6177 | 0 | -2702.6327 | -9.43 | -2702.6478 | -18.86 |

**Table ST2**: *Values for Lowest Energy Geometries without Dihedral Constraint for Au-**Si4**-Au (Figure 4c)*

| Au-Au Distance (Å) | Elongation (Å) | Dihedral Config. | [Au-**Si4**-Au]$^{2+}$ Total Energy (Hartrees) | Si-Si-Si-Si Dihedral | Me-S-CH$_2$-SiMe$_2$- ($\omega_1$) | Me-S-CH$_2$-SiMe$_2$- ($\omega_2$) | Au-S bond length (Å) | Neutral Au-**Si4**-Au Rel. Tunnel Coupling |
|---|---|---|---|---|---|---|---|---|
| 13.25 | -0.50 | A-A | -2702.6582 | 161.5 | -167.9 | -177.9 | 2.34 | 1.018 |
| 13.50 | -0.25 | A-A | -2702.6591 | 162.9 | 166.3 | -171.9 | 2.34 | 1.013 |
| 13.75 | 0.00 | A-A | -2702.6591 | 168.6 | 177.5 | -178.5 | 2.34 | 1.000 |
| 14.00 | 0.25 | A-A | -2702.6588 | 171.6 | 172.3 | -176.0 | 2.35 | 0.962 |
| 14.25 | 0.50 | O-A | -2702.6592 | 169.1 | -88.6 | 176.3 | 2.34 | 1.034 |
| 14.50 | 0.75 | O-A | -2702.6589 | 169.1 | -91.6 | 176.6 | 2.35 | 1.018 |
| 14.75 | 1.00 | O-A | -2702.6585 | 170.5 | -92.2 | 173.6 | 2.35 | 0.974 |
| 15.00 | 1.25 | O-O | -2702.6586 | 172.6 | 89.8 | -86.4 | 2.35 | 1.346 |
| 15.25 | 1.50 | O-O | -2702.6594 | 170.7 | 88.4 | -87.3 | 2.35 | 1.286 |
| 15.50 | 1.75 | O-O | -2702.6597 | 169.0 | 88.8 | -89.3 | 2.36 | 1.343 |
| 15.75 | 2.00 | O-O | -2702.6589 | 166.1 | 90.4 | -91.4 | 2.36 | 1.328 |
| 16.00 | 2.25 | O-O | -2702.6577 | 164.6 | 91.1 | -92.1 | 2.37 | 1.346 |
| 16.25 | 2.50 | O-O | -2702.6554 | 165.0 | 91.6 | -92.0 | 2.38 | 1.370 |
| 16.50 | 2.75 | O-O | -2702.6522 | 165.8 | 91.8 | -91.8 | 2.40 | 1.343 |
| 16.75 | 3.00 | O-O | -2702.6578 | 167.3 | 91.2 | -91.1 | 2.43 | 1.403 |

**Table ST3**: *Values for Lowest Energy Geometries of Au-**C6**-Au (Supplementary Figure S5)*

| Au-Au Distance (Å) | Elongation (Å) | [Au-**C6**-Au]²⁺ Dihedral Config. | Total Energy (Hartrees) | Me-S-CH₂-CH₂- (ω₁) | Me-S-CH₂-CH₂- (ω₂) | Au-S bond length (Å) | Neutral Au-**C6**-Au Rel. Tunnel Coupling |
|---|---|---|---|---|---|---|---|
| 10.63 | -0.50 | A-A | -1382.4727 | 170.4 | -170.5 | 2.34 | 1.107 |
| 10.88 | -0.25 | A-A | -1382.4735 | 174.1 | -173.9 | 2.34 | 1.058 |
| 11.13 | 0.00 | A-A | -1382.4737 | 178.1 | -178.3 | 2.35 | 1.000 |
| 11.38 | 0.25 | A-A | -1382.4736 | 177.5 | -177.2 | 2.35 | 0.983 |
| 11.63 | 0.50 | O-A | -1382.4733 | 78.3 | 175.8 | 2.35 | 0.939 |
| 11.88 | 0.75 | O-A | -1382.4734 | 79.2 | -179.0 | 2.35 | 0.860 |
| 12.13 | 1.00 | O-A | -1382.4730 | 79.2 | -172.6 | 2.35 | 0.913 |
| 12.38 | 1.25 | O-A | -1382.4725 | 80.2 | -163.8 | 2.35 | 0.882 |
| 12.63 | 1.50 | O-O | -1382.4713 | 90.9 | -71.4 | 2.34 | 0.973 |
| 12.88 | 1.75 | O-O | -1382.4728 | 83.4 | -75.2 | 2.34 | 0.943 |
| 13.13 | 2.00 | O-O | -1382.4735 | 77.3 | -77.3 | 2.35 | 0.935 |
| 13.38 | 2.25 | O-O | -1382.4721 | 76.1 | -75.8 | 2.37 | 0.950 |
| 13.63 | 2.50 | O-O | -1382.4688 | 74.9 | -74.6 | 2.40 | 0.896 |
| 13.88 | 2.75 | O-O | -1382.4639 | 76.7 | -76.3 | 2.43 | 0.933 |
| 14.13 | 3.00 | O-O | -1382.4573 | 76.2 | -76.3 | 2.47 | 1.004 |

## VI. References

1.  Chang, S., He, J., Zhang, P., Gyarfas, B. & Lindsay, S. Gap distance and interactions in a molecular tunnel junction. *J. Am. Chem. Soc.* **133,** 14267–9 (2011).

2.  Frei, M., Aradhya, S. V, Koentopp, M., Hybertsen, M. S. & Venkataraman, L. Mechanics and chemistry: single molecule bond rupture forces correlate with molecular backbone structure. *Nano Lett.* **11,** 1518–23 (2011).

3.  Lin, J. & Beratan, D. N. Tunneling while Pulling: The Dependence of Tunneling Current on End-to-End Distance in a Flexible Molecule. *J. Phys. Chem. A* **108,** 5655–5661 (2004).

4.  Lafferentz, L. *et al.* Conductance of a single conjugated polymer as a continuous function of its length. *Science* **323,** 1193–7 (2009).

5.  Fan, F.-R. F. *et al.* Charge transport through self-assembled monolayers of compounds of interest in molecular electronics. *J. Am. Chem. Soc.* **124,** 5550–60 (2002).

6.  Klausen, R. S., Widawsky, J. R., Steigerwald, M. L., Venkataraman, L. & Nuckolls, C. Conductive molecular silicon. *J. Am. Chem. Soc.* **134,** 4541–4 (2012).

7.  Piqueras, M. C., Crespo, R. & Michl, J. The Transoid, Ortho, and Gauche Conformers of Decamethyl- n -tetrasilane, n -Si 4 Me 10 : Electronic Transitions in the Multistate Complete Active Space Second-Order Perturbation Theory Description. *J. Phys. Chem. A* **107,** 4661–4668 (2003).

8.  Fogarty, H. a, Imhof, R. & Michl, J. Magnetic circular dichroism of peralkylated tetrasilane conformers. *Proc. Natl. Acad. Sci. U. S. A.* **101,** 10517–22 (2004).

9.  George, C. B., Ratner, M. a & Lambert, J. B. Strong conductance variation in conformationally constrained oligosilane tunnel junctions. *J. Phys. Chem. A* **113,** 3876–80 (2009).

10. Michl, J. & West, R. Conformations of linear chains. Systematics and suggestions for nomenclature. *Acc. Chem. Res.* **33,** 821–3 (2000).

11. Kobayashi, T. & Pannell, K. H. Synthesis of (chloromethyl)silanes by the low-temperature reaction of chlorosilanes and in situ generated (chloromethyl)lithium in tetrahydrofuran. *Organometallics* **10,** 1960–1964 (1991).

12. Kobayashi, T. & Pannell, K. H. A general, high-yield reaction for the formation of (chloromethyl)oligosilanes. *Organometallics* **9,** 2201–2203 (1990).

13. Aradhya, S. V, Frei, M., Hybertsen, M. S. & Venkataraman, L. Van der Waals interactions at metal/organic interfaces at the single-molecule level. *Nat. Mater.* **11,** 872–6 (2012).

14.     Hay, P. J. & Wadt, W. R. Ab initio effective core potentials for molecular calculations. Potentials for K to Au including the outermost core orbitals. *J. Chem. Phys.* **82,** 299 (1985).

15.     Park, Y. S. *et al.* Contact chemistry and single-molecule conductance: a comparison of phosphines, methyl sulfides, and amines. *J. Am. Chem. Soc.* **129,** 15768–9 (2007).